Microstructure and arc erosion behavior of WC/CuCr30 composites based on nano-Cr precipitation

GUO, Xiuhua, SONG, Kexing, DUAN, Kaiyue, LUO, Quanshun <http://orcid.org/0000-0003-4102-2129>, LI, Kai and MIAO, Xiaojun

Published version

GUO, Xiuhua, SONG, Kexing, DUAN, Kaiyue, LUO, Quanshun, LI, Kai and MIAO, Xiaojun (2024). Microstructure and arc erosion behavior of WC/CuCr30 composites based on nano-Cr precipitation. Vacuum: 112954.

Microstructure and arc erosion behavior of WC/CuCr30 composites based on nano-Cr precipitation

Xiuhua Guo[a], Kexing Song[a,b*], Kaiyue Duan[a], Quanshun Luo[c], Kai Li[d], Xiaojun Miao[d]

a. Henan Key Laboratory of Non-ferrous Materials Science & Processing Technology, Henan University of Science and Technology, Luoyang 471023, China

b. Henan Academy of Sciences, Zhengzhou 450052, China

c. Materials and Engineering Research Institute, Sheffield Hallam University, Sheffield S1 1WB, UK

d. Henan Pinggao Electric Co Ltd, Pingdingshan 467001, China

Abstract:

CuCr alloys with high contact performance for medium and high voltage vacuum circuit breakers are becoming increasingly urgent. In this work, WC/CuCr30 composites were prepared by SPS process, and nanometer-sized precipitated Cr phases were obtained by subsequent heat treatment. The microstructure and arc erosion behavior were investigated. The results show that nano-Cr phase precipitated in copper matrix can effectively improve the interfacial bonding strength between the Cu matrix and WC particles, and part of the precipitated nano-Cr phase is combined with the C element in WC to form nano-$Cr_{23}C_6$. Both nanophases can improve the resistance to dislocation and sub-grain boundary movement in the deformation process of WC/CuCr30 composite, thus improving the hardness of the copper matrix with a slight decrease in electrical conductivity. The results of electrical contact show that the addition of WC particles and nano-Cr precipitates can not only extend contact life of CuCr material, but also help to disperse the arc to avoid concentrated erosion. The presence of $Cr_{23}C_6$ phase around WC particles effectively improves the interfacial bonding between Cu phase and WC phase and reduces the probability of pore existence at the interface, which is beneficial to vacuum breaking performance.

Keywords: WC/CuCr30 composites, nano-Cr precipitate, solution and aging heat treatment, arc erosion, welding resistance

1 Introduction

CuCr alloys with high Cr content (20-50 wt%) have become the preferred material for medium voltage high power vacuum circuit breaker contacts due to their excellent characteristics such as low resistance and high current interrupting capability, high voltage strength and low cut-off current [1-5]. With the development of vacuum circuit breaker towards miniaturization, high power and high reliability, the service life and stability requirements of contacts are increasingly higher [6-8].

In recent years, researchers have focused on adding a third strengthening phase to improve the arc erosion resistance of CuCr contact materials, such as Mo[9], W[10], CeO[11], Cr_2O_3[12], WC[13], etc. Liang found that the welding force of Cu30Cr10W composites was reduced when nano-CeO_2 doped with graphene oxide (GO) was introduced [11]. Han studied the effect of Cr_2O_3 during in-situ preparation of homogeneous CuCr50 alloy by high temperature self-propagating synthesis metallurgy and found that the relative density of prepared CuCr alloy increased from 90.9% to 98.5% with the increase of Cr_2O_3 content [12]. Duan discovered that micron-sized WC particles in CuCr30 composites helped increase the melt pool area and prevent the continuous deepening of the melt pool of CuCr contact in the arc erosion process [13]. Chang found that the average welding force of CuCr-W-C alloys was reduced by more than 50% compared to that of the Cu_{50} Cr_{50} alloy [14]. Cho found that the Cu-Cr-Mo alloy fabricated by an

infiltration method had better physical properties than that produced by a sintering process [15]. Zhang reported that the deposition of a Cu-Cr-W coating on a pure Cu substrate could improve microhardness and tribological properties [10]. According to the Cu-Cr binary phase diagram, Cu and Cr have very little solubility in each other, implying that a mono-phase CuCr alloy would be thermodynamically meta-stable. Therefore, a combined process of solutioning and aging treatments could be an effective method to modify the material structure and subsequently optimize the properties [16-18]. Shan improved the high temperature mechanical performance of Cu-Cr alloy by introducing nano-sized Cr residual precipitates into the matrix through the combination of mechanical alloying and spark plasma sintering [16]. Zuo found that a remarkable improvement in both mechanical and physical properties of W/CuCr0.5 composites is attributable to the synergistic effect of the concrete skeleton of particulate and fibrous W together with the abundant coherent Cr precipitates in Cu matrix [17].

In this work, micro-WC particles were introduced into Cu-Cr composite as a third reinforcement. The WC/CuCr30 composites were prepared by spark plasma sintering (SPS) and Cu-2wt.%Cr alloy powders were selected to replace pure Cu powder, and the precipitated nanometer Cr phases were obtained by heat treatment of solid solution and aging. The effects of micro-WC particles and nano-Cr precipitation on microstructure evolution and compressive properties of WC/CuCr30 composites were analyzed and discussed. The arc erosion resistance of WC/CuCr30 composites at different electric currents, such as arc energy, welding force and mass change was investigated, and the mechanisms of electrical contact properties improved by micro-WC particles and nano-Cr precipitation are outlined.

2 Materials and Methods

2.1 Raw materials

The starting materials were Cu-2wt.%Cr alloy powder (purity 99.9 wt%, particle size 40 μm, Hunan Huabang Powder Materials Co., Ltd), Cr powder (purity 99.9 wt%, particle size 75 μm, Xi'an Sirui Advanced Copper Alloy Technology Co., Ltd), and WC powder (purity 99.9 wt%, particle size 10 μm, Shanghai Puwei Applied Materials Technology Co., Ltd). The morphologies and XRD patterns of raw powders are shown in Fig. 1. Fig.1(a)(a_1) shows the Cu-2wt.%Cr alloy powders with an average particle size of 40 μm, which have the fcc structure and a lattice parameter of a = 3.621 nm. Fig.1(b)(b_1) shows Cr powders with a bcc structure and a lattice parameter of a = 2.886 nm, which are 75 μm in average size with regular block structure. Fig.1(c)(c_1) shows WC powders with a hexagonal crystal structure and a lattice parameter of a = 2.906 nm, and the powders are in the shape of round granules with an average size of 10 μm.

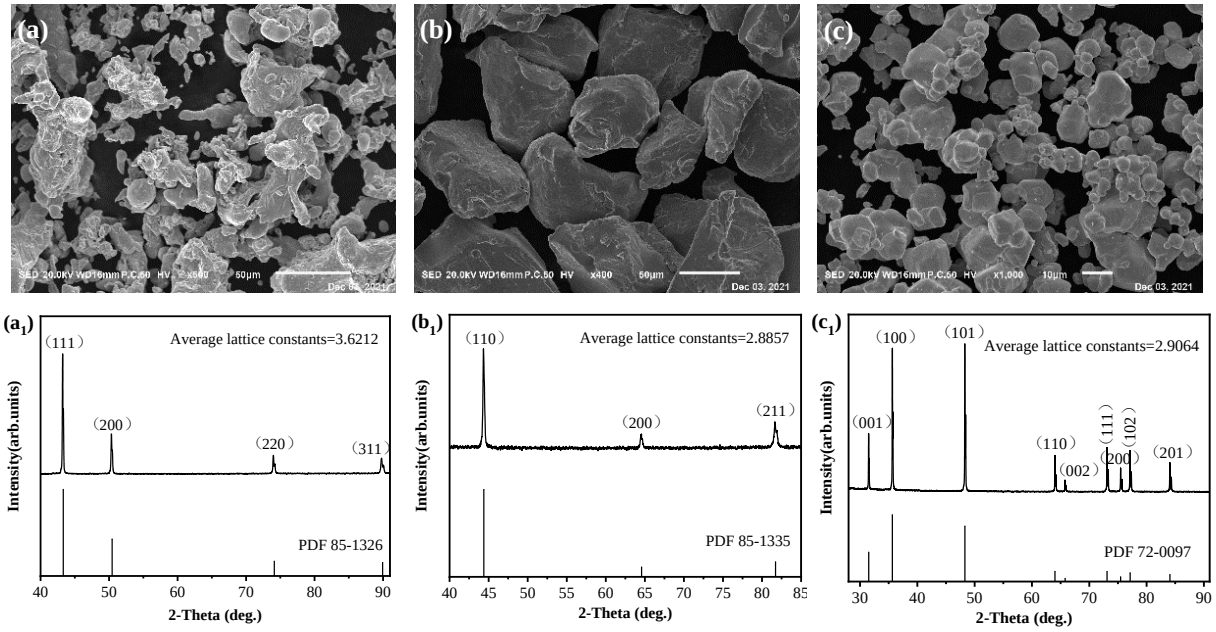

Fig. 1. Morphologies and XRD patterns of raw powders. (a)(a_1) Cu-2wt.%Cr, (b)(b_1) Cr, (c)(c_1) WC

2.2 Preparation of WC/CuCr30 composites

A powder metallurgy process was applied to fabricate the WC/CuCr30 composites. Firstly, the WC particles, Cu-2wt.%Cr alloy powders and micro-Cr powders were ball-milled using a planetary ball milling machine (YXQM-8L, Changsha Miqi Instrument Equipment Co., Ltd, China), with a mass ratio of 6:64:30, and then milled for 24 h at 40 r/min with the ball-to-powder ratio of 5:1. Secondly, the mix powders were compressed and sintered at 950°C for 10 min under 40 MPa in vacuum conditions of 1.1 Pa, using a fast hot-pressure sintering furnace (FHP-828, Shanghai Hateng Electric Furnace Equipment Co. , Ltd., China). The block samples produced were 20 mm in diameter and 10 mm in length. Thirdly, the sintered compact was heated to hold at 900°C for 1h and then aged at 450°C for 3h in an SX2-2.5-10 box type resistance furnace. Moreover, a CuCr30 compact composed of Cu powders (70 wt%) and Cr powders (30 wt%) was also prepared by the same fabrication process to serve as a reference sample.

2.3 Microstructure characterization and property testing

The phase identification of raw powders was evaluated by X-ray diffractometer (XRD, D8-Advance). The microstructure and erosion surface of WC/CuCr30 composites and CuCr30 composites were characterized by scanning electron microscopy (SEM, JSM-5610LV, JEOL). The element distribution of composites was acquired by energy dispersive spectrometer (EDS) attached to field emission scanning electron microscope (FE-SEM, JSM-7800F, JEOL). The nano phases distribution and dislocations in composite were characterized on the transmission electron microscope (TEM, JEM-2100, JEOL). The relative density was measured utilizing the Archimedean method. The hardness was tested on a 320HBS-3000 Brinell hardness tester under the load 250 kg. The electrical conductivity was measured on a Sigma 2008B1 digital conductivity meter. To ensure the accuracy of these measurements, each test was repeated five times to obtain the mean value and deviation.

2.4 Electrical contact testing

Electrical contact tests were carried out using an electrical contact tester (JF04C, Kunming Institute of Precious Metals, China) in atmospheric environment, as schematically shown in Fig. 2. The anode and cathode corresponded

to the movable contact and stationary contact, respectively. And the anode and cathode with a diameter of 3.8 mm and a length of 10 mm were machined from the as-prepared specimens. Each contact pair was performed 5000 times under a voltage of 24 VDC and currents of 15 A, 20 A and 25 A, respectively, with the operation frequency of 1 Hz, electrode gap of 2 mm and contact force of 50 cN. Data on arcing duration, arc energy, and welding force was automatically recorded by the system. Five contact samples were tested to ensure the repeatability of the test. A scanning electron microscope (SEM, JSM-5610LV, JEOL, Japan) was used to observe the arc erosion morphologies of the dual contacts.

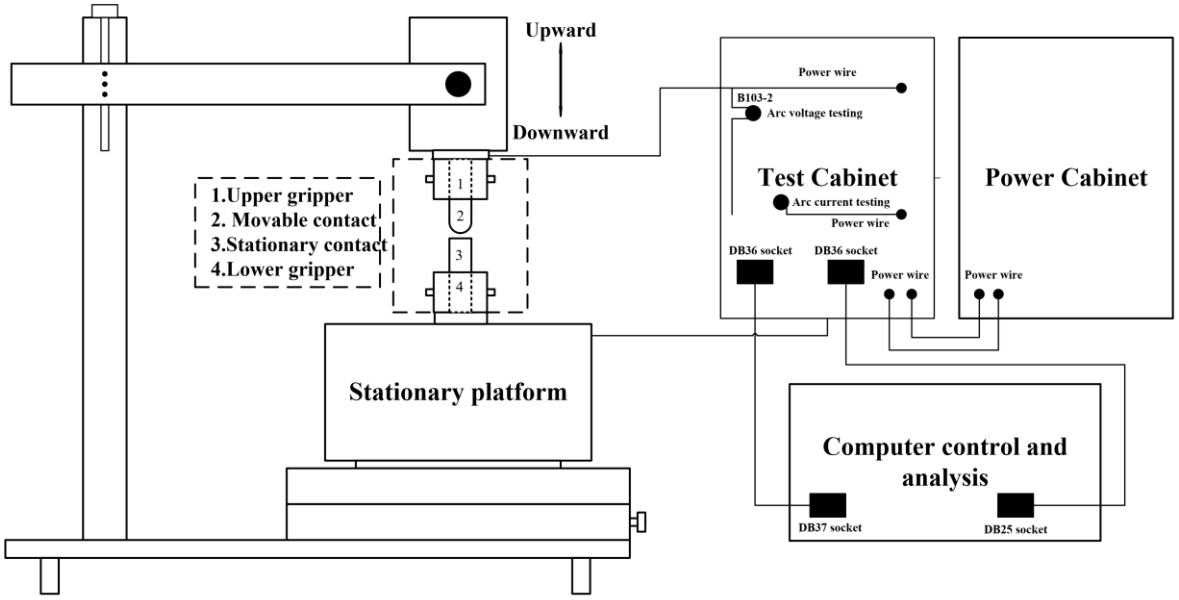

Fig. 2. Schematic of JF04C electric contact material testing system.

3 Results and discussion

3.1 Microstructure and comprehensive properties of WC/CuCr30 composites

Fig.3 shows the microstructure of the fabricated WC/CuCr30 and CuCr30 composites. Among the dispersed reinforced particles, the Cr phases show black spots and WC particles show the smaller white spots in Fig.3(a). The Cr and WC particles both exhibit uniform distribution in the copper matrix, whereas the compact is dense showing no cracks and pores. To further prove the elements and their distribution status, the energy spectrum analysis and elemental mapping of Cu, Cr, WC in WC/CuCr30 composite are shown in Fig.4. As seen from Fig. 4, the WC phase and Cr phase are dispersed uniformly in the copper matrix. And the content of Cr is 29.6 wt.%, and that of W is 6.2 wt.%, which is consistent with the designed content of 30 wt.%Cr and 6 wt.%WC.

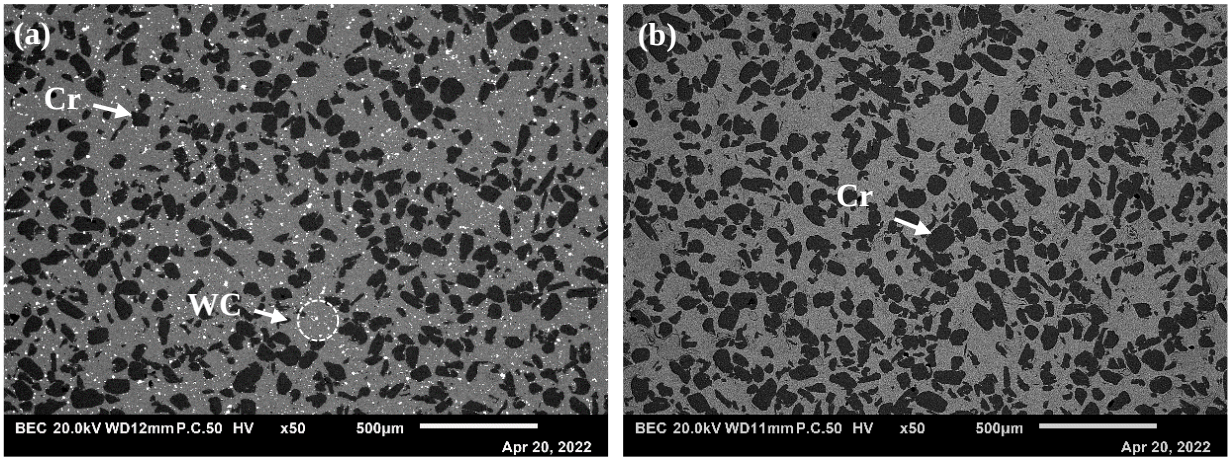

Fig. 3. SEM images of composites after aging heat treatment. (a) WC/CuCr30, (b) CuCr30

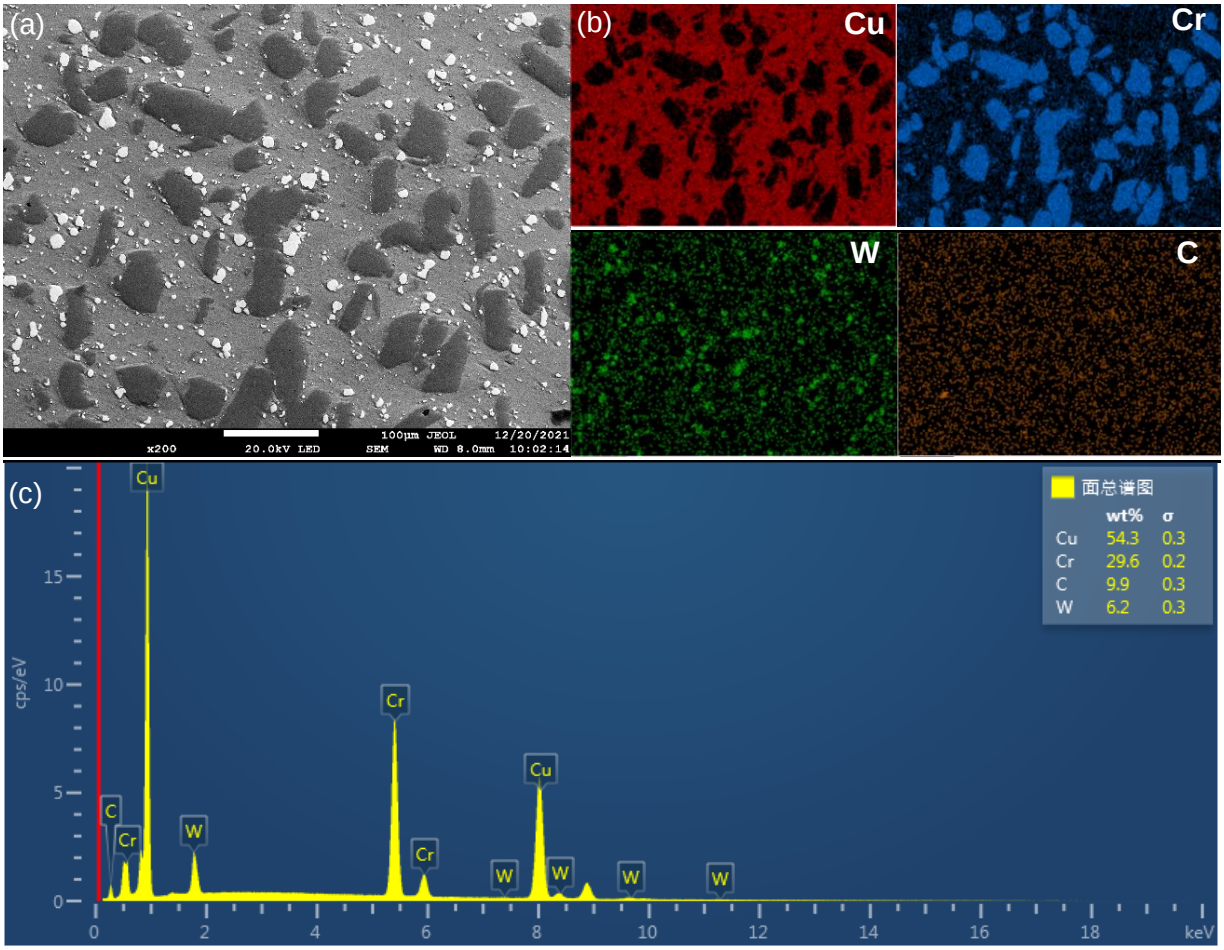

Fig. 4. SEM image and EDS analysis WC/CuCr30 composite

Fig.5 and Fig. 6 show line scan images and elemental analysis of Cr phase and WC phase, respectively. As known, the binding force between metal phase and metal phase is greater than the binding force between metal and ceramic particle. As seen Fig.5(b), the Cr phase has a well interface bonding with copper matrix, due to the metallic phase of both Cu matrix and Cr phase. As seen in Fig.6, the line scan shows an intermediate zone between the WC and the Cu matrix, indicating diffusion of Cr, Cu and WC at the WC-Cu interface, and there is a narrow transition zone of "Cr" between Cu and WC. It proves that the layer of "Cr" phase around the WC particles is helpful to

improve the interface bonding between the Cu phase and the WC particles.

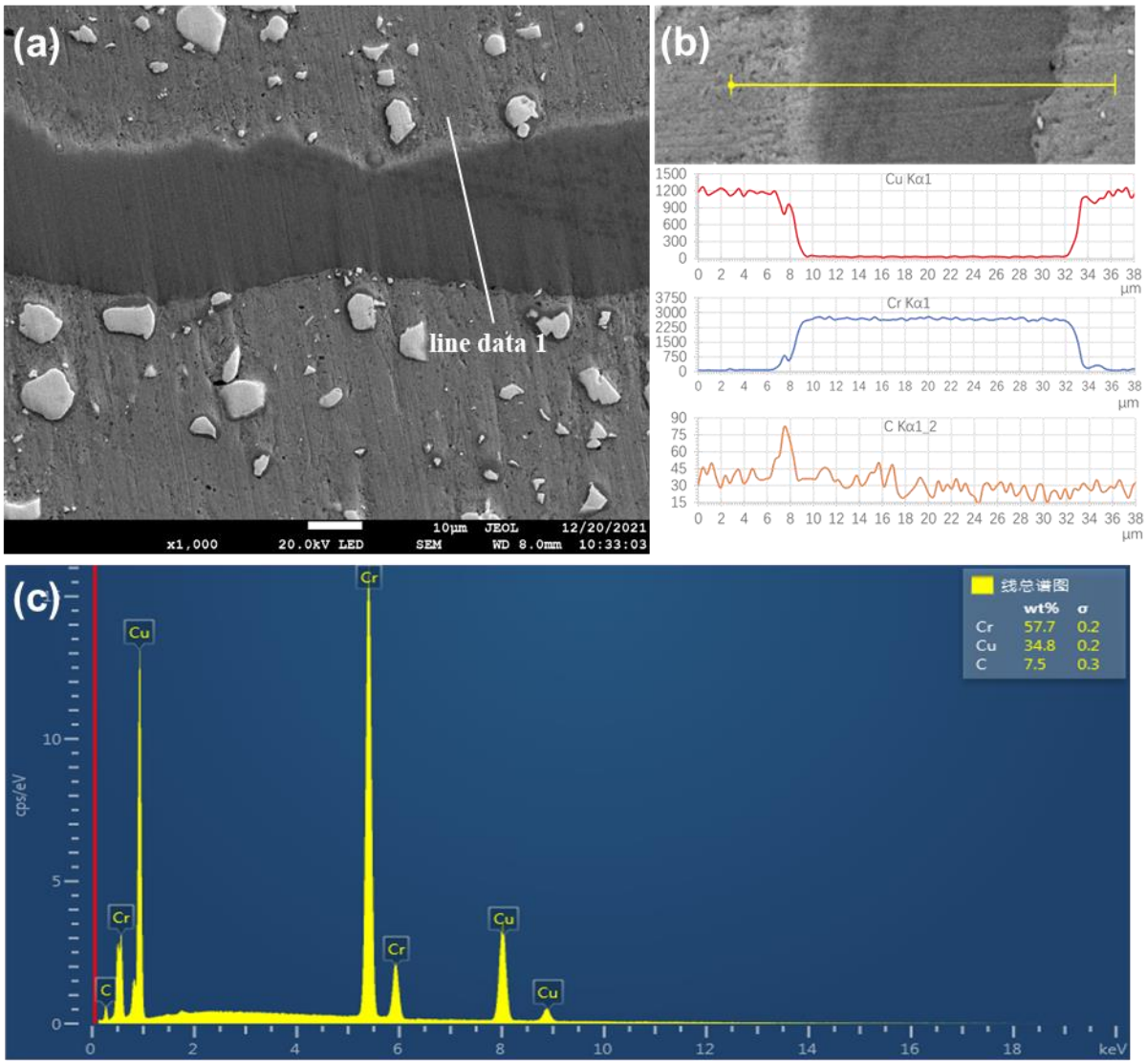

Fig. 5. SEM image and Cr line scans spectrum of WC/CuCr30 contact material.

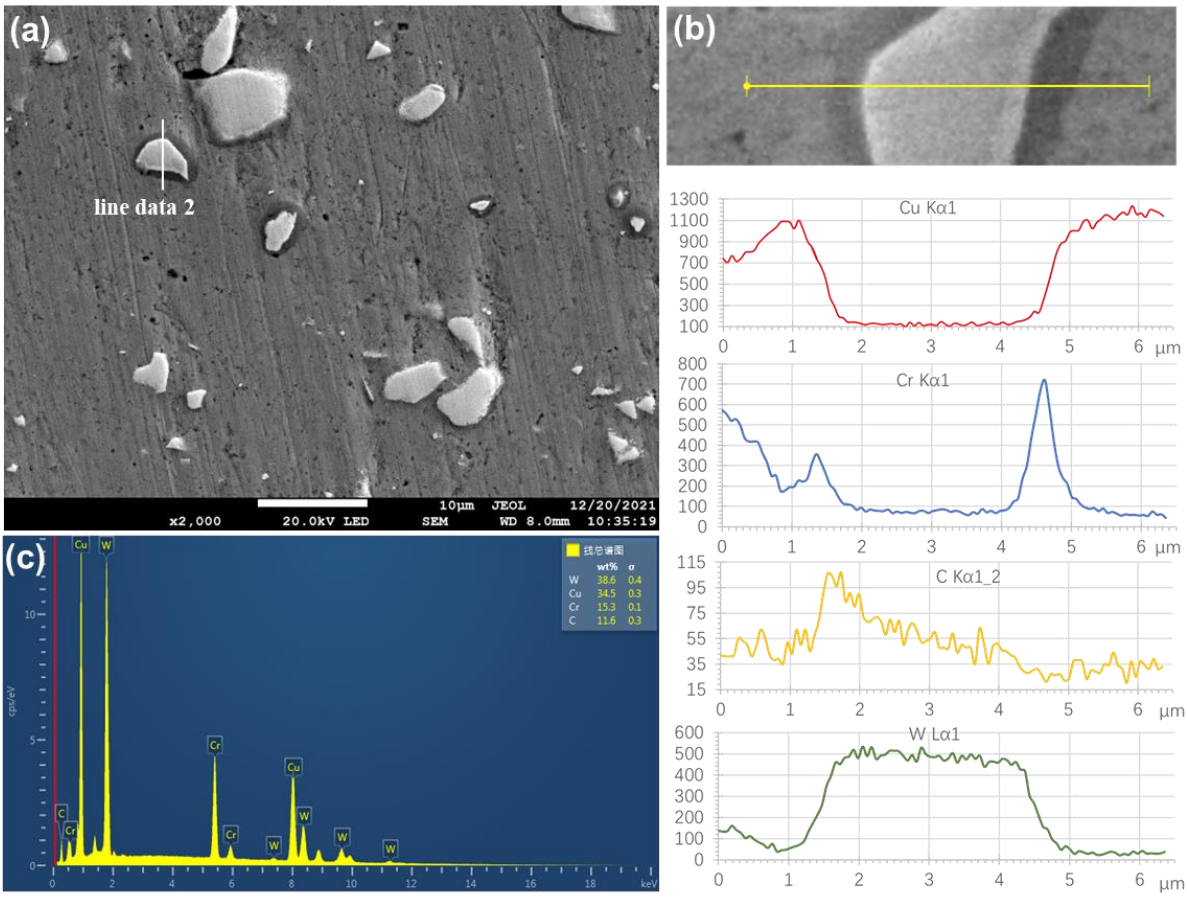

Fig. 6. SEM image and WC line scans spectrum of WC/CuCr30 contact material.

Fig. 7 shows a TEM bright field (BF) image and three patterns of related selected area diffraction (SAD) of the WC/CuCr30 composite. As seen, the SAD patterns match the Cu phase, $Cr_{23}C_6$ phase (mark B) and Cr phase (mark C) in Fig. 7(a), respectively. The characterization shows that the nano-Cr particles precipitate during heat treatment, and compounds of $Cr_{23}C_6$ are also formed through chemical reactions. It is because the binding force between element C and element Cr is greater than that between element C and element W, and the micron-scale Cr phase in the matrix and precipitated nano-Cr phase are easy to react with element C in WC to generate phase $Cr_{23}C_6$ [19]. Combined with Fig.6, the "Cr" phases gather around WC particles, forming a layer of Cr, and part of Cr phase is combined with the C element in WC to form $Cr_{23}C_6$. The Cr element is mainly precipitated in two forms in the alloy powder, one is mainly precipitated in the form of nano-Cr on the Cu matrix, and the other is mainly precipitated around the WC particles. As seen in Fig.7(b), the precipitated nano-Cr particles and compounds of $Cr_{23}C_6$ are mostly pinned at grain boundaries and interfaces with particle sizes ranging from 20nm to 100 nm. According to the Smith-Zener pinning principle [20], the pinning effect can effectively inhibit grain boundary migration and grain growth, improve the interfacial bonding strength between the Cu matrix and WC particles.

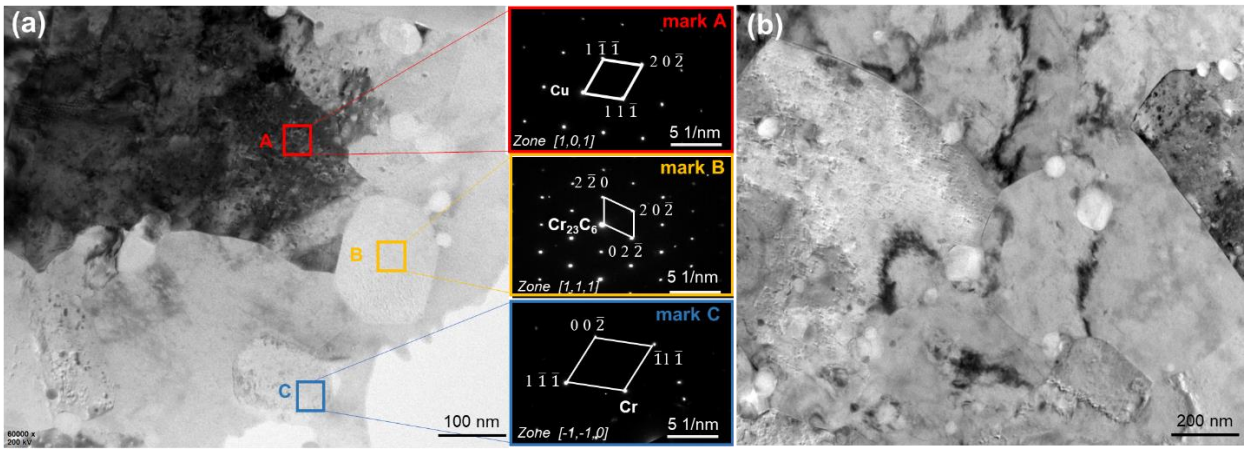

Fig.7. TEM image of WC/CuCr30 composite.

(a) SAD of the WC/CuCr30 composite; (b) distribution of nano Cr phases and $Cr_{23}C_6$ compounds

Table 1 shows the comprehensive properties of WC/CuCr30 and CuCr30 composites at different states. The density of WC/CuCr30 and CuCr30 composites in both hot pressed and aged states are above 99%. After heat treatment, the hardness of WC/CuCr30 and CuCr30 composites significantly increases about 14%, and the electrical conductivity increases smoothly. As seen in Table 1, the addition of WC particles obviously enhanced hardness of CuCr30 composite, especially after aged heat treatment, the hardness of WC/CrCr30 composite reaches 145.4 HB. There are two reasons for the enhancement. Firstly, WC ceramic particles not only have thermal and chemical stability (melting point 2993 K), but also have good wettability with copper, which can substantially improve the mechanical properties of the copper [21]. Secondly, nano-Cr phase participated and nano compounds of $Cr_{23}C_6$ are also formed through chemical reactions in copper matrix. Both nano phases can improve the resistance of dislocation and sub-grain boundary movement in the deformation process of WC/CuCr30 composite, thus improving the hardness of copper matrix. Fig. 8 shows the dislocation crossing and entanglement caused by the pinned dislocation of Cr nanoparticles. The introduction of nanoscale Cr phase can hinder the resistance of dislocations and sub-grain boundary movement during the deformation process of WC/CuCr30 composite materials, thereby increasing the hardness of the copper matrix. However, the addition of WC particles leads to more crystal defects in copper matrix, damages the lattice structure integrity of copper matrix, obstructs electron motion, and increases electron scattering, resulting in the light decrease of conductivity of WC/CuCr30 composite, as seen in Table 1. Deng constructed a model of the relationship between interface density and hardness and resistivity of composites, and its expression is as follows [22]:

$$HV=660S_v^{0.5}+108 \quad (1)$$

$$\rho=\rho_0\ [1+3al_0\ (1-p)/4(8/\pi S_v-d)] \quad (2)$$

Where, S_v is interface density, nm^2/nm^3; ρ_0 is the resistivity without interface scattering; p is the probability of an electron scattering elastically at the interface (the elastic scattering factor); $(1-p)$ is the probability of an electron scattering inelastically at the interface; l_0 is the mean free path of electrons. As seen from the equations (1) and (2), the greater number of grain boundaries, the greater the crystal deformation resistance. The grain boundaries will increase the scattering probability of electrons and increase the resistivity. The introduction of WC reinforcement phase particles increases the interface density, and the nano Cr phases can hinder dislocation slip, both aspects will make WC/CuCr30 with a higher hardness and a lower conductivity than CuCr30.

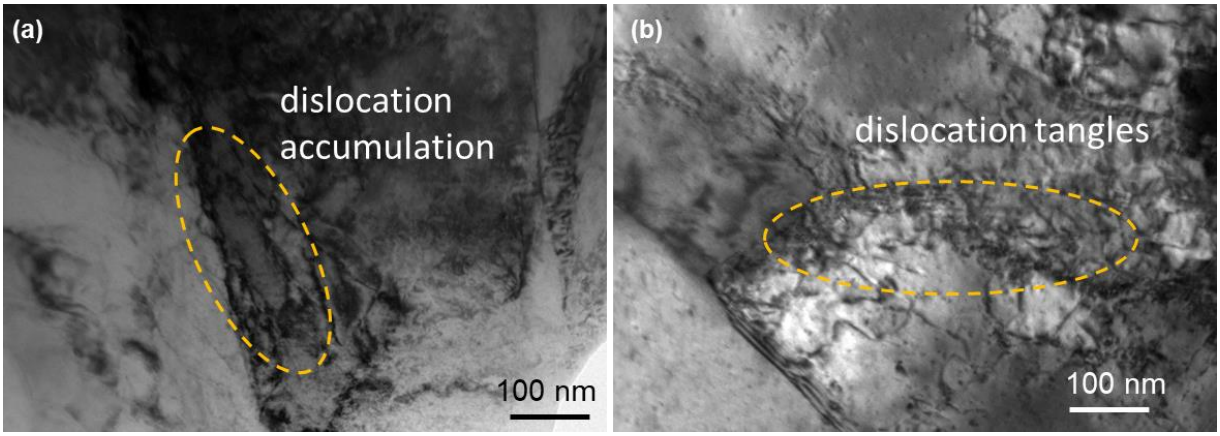

Fig. 8. TEM image of dislocations in WC/CuCr30 composites. (a) dislocations accumulation; (b) dislocations tangles.

Table 1 Relative density, hardness, and electrical conductivity of WC/CuCr30 composites.

Composite	Relative density (%)		Hardness (HB)		Electrical conductivity (%IACS)	
	Hot- pressed	Heat treatment	Hot-pressed	Heat treatment	Hot-pressed	Heat treatment
WC/CuCr30	99.18	99.17	128.17±1.48	145.4±2.7	47.19±0.47	48.92±0.15
CuCr30	99.21	99.24	123.40±1.14	140.8±1.48	49.03±0.27	52.08±0.26

3.2 Arc erosion behavior of WC/CuCr30 composites

3.2.1 Arc energy, arc duration and arc stability

Fig.9 shows the average arc energy and arc duration of heat-treated WC/CuCr30 and CuCr30 composites under different current conditions. As seen, the average arc energy and arc duration of WC/CuCr30 composites are significantly lower than that of CuCr30 composites, which indicates that the addition of WC particles can significantly reduce the arc energy and arc duration of the CuCr30 composites. Especially under a low current of 15A, the arc energy and arc duration of WC/CuCr30 composites are almost half of CuCr30 composites, while reaching the considerable degree of CuCr30 composites under a high current of 25A. It needs to be pointed out that only 3835 operations were performed for CuCr30 composite due to failure caused by welding, which lead to a smaller difference of arc energy and are duration between WC/CuCr30 composite and CuCr30 composite under a high current of 25A.

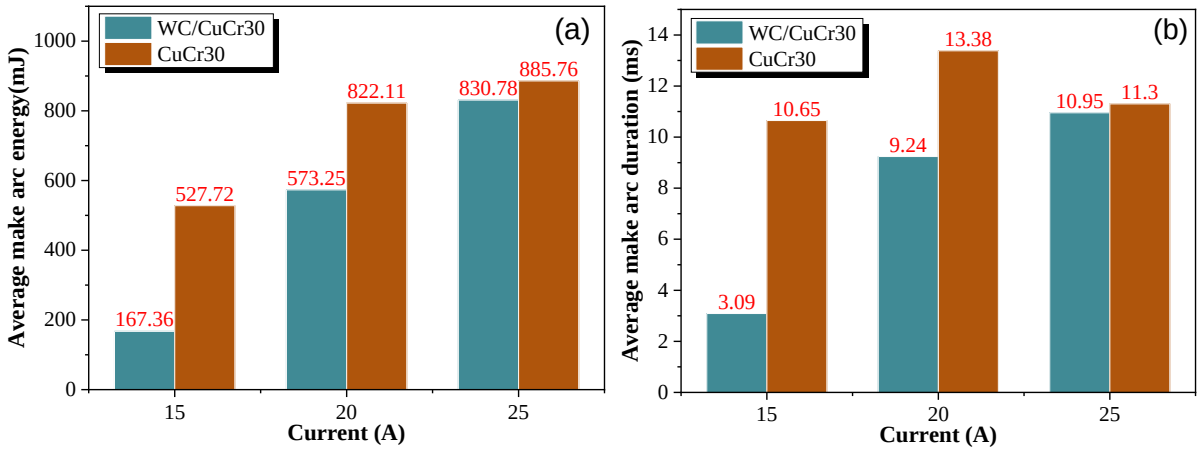

Fig. 9. Average arc energy and arc duration of WC/CuCr30 and CuCr30 composites under different currents. (a) make arc energy (b) make arc duration

Fig.10 shows the variation of arc energy and arc duration of WC/CuCr30 and CuCr30 composites against operation times. The make arc energy shows the same changing trend with its make arc durations. The make arc energy of CuCr30 composites show smooth variation at first, followed by a sharp increase with violent fluctuations. The make arc energy of the WC/CuCr30 are much lower than that of the CuCr30 composites with smaller volatility against operation times, especially at high current of 25A. The results indicate that the WC/CuCr30 composite has better stability against arc erosion. At 15 A, the make arc energy of WC/CuCr30 composites are the lowest, which are equivalent to 31.7% and 47.5% of CuCr30 composites. At 20 A, the make arc energy of WC/CuCr30 composites decreased by 30.3% and 51.1% compared with CuCr30 composites. Meantime, it needs to be pointed out that only 3835 operations were performed for CuCr30 composite due to failure caused by welding, as seen in Fig.10(a)(a_1). The influence of current on arc energy is mainly reflected in arc current, the arc energy increases with the increasing of arc injection current [23-25]. When the current is 15 A, on one hand, the introduction of WC particles can better disperse the arc and avoid concentrated arc erosion, and the ability of WC particles to disperse the arc plays a dominant role; On the other hand, low current generates less heat, heat is easy to dissipate in WC/CuCr30 composites, and the effect of current on arc energy is relatively low. When the current increases to 25 A, the arc energy and heat are very high, and the limited heat conduction capacity of WC/CuCr30 composite is not enough to fully dissipate heat, which intensifies the arc erosion on surface of contacts, and the heat conduction performance of WC/CuCr30 composite will play a dominant role.

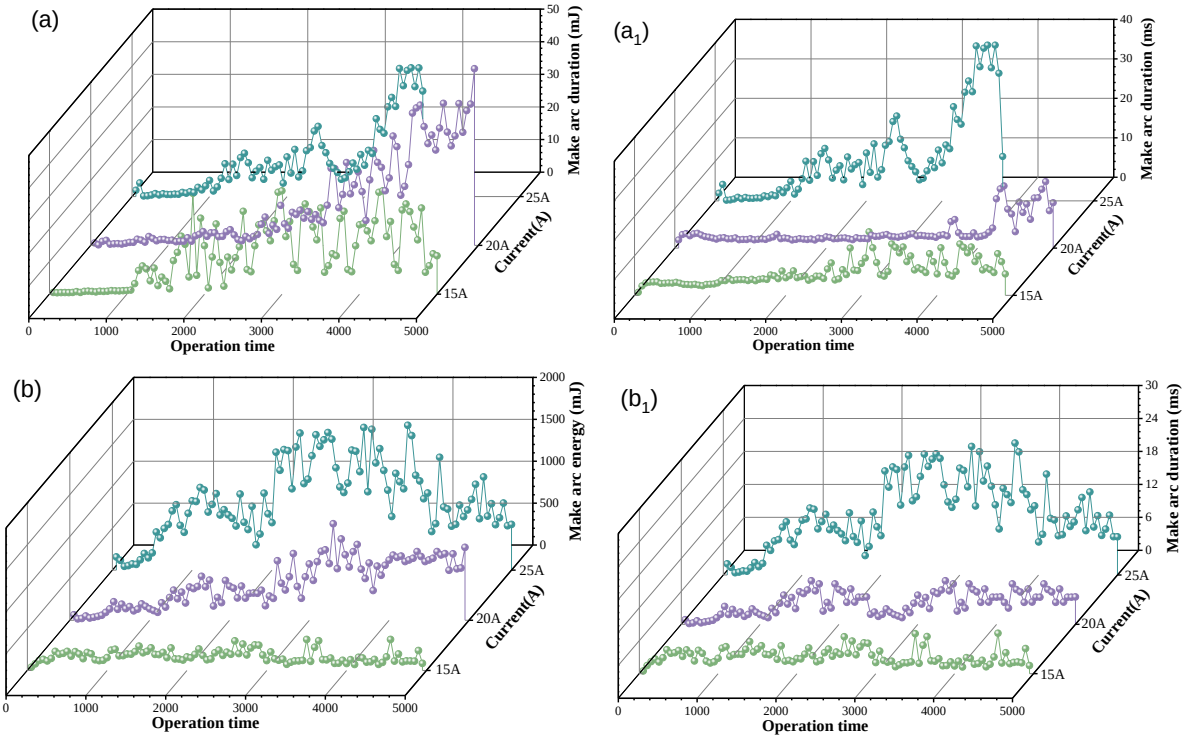

Fig.10 Variation curves of arc energy and arc duration of WC/CuCr30 and CuCr30 composites under different currents. (a)(a1) CuCr30 composite, (b)(b1) WC/CuCr30 composite

3.2.2 Welding force and material transfer analysis

Fig.11 and Fig.12 show the average welding force and the variation of welding force of WC/CuCr30 and CuCr30 composites under different currents. The welding force of WC/CuCr30 composite increases with the

increase of current, and WC/CuCr30 composites have better welding resistance and stability than that of CuCr30 composites. At 15 A and 20 A, the average welding force of WC/CuCr30 composite is 9.08% and 9.00% lower than that of CuCr30 composite, respectively, and the fluctuation of welding force is smaller than CuCr30. At 25 A, it can be seen from Fig. 12(a) that operation times of WC/CuCr30 composite reaches 5000, while the operations times of CuCr30 composite is only 3835 due to failure. The results improve that the addition of WC and nano-Cr precipitation extend the service life of CuCr30 composite. The contact welding is always associated with arc erosion during the service, resulting in the failure of the contact pairs. Fig.13 shows mass changes of WC/CuCr30 and CuCr30 composites under different currents. For WC/CuCr30 composite, the mass transfer is from cathode to anode, and the mass loss increases with increasing of current. At low current of 15 A, the mass changes of the anode and cathode of WC/CuCr30 composite reaches the lowest, which were + 0.3mg and -0.3mg, respectively. However, the transfer direction of CuCr30 composite occurred from anode to cathode, the anode and cathode mass loss of CuCr30 material were -0.13 mg and +0.34 mg, respectively. With the current increase to 20 A and 25 A, both CuCr30 and WC/CuCr30 composite transfer from cathode to anode, and the mass loss increase with increasing of current. Especially for WC/CuCr30 materials, the mass loss of both anode and cathode is much more than that of CuCr30 composite. The results show that the CuCr30 composites have less material transfer than WC/CuCr30 materials at high currents. It needs to be pointed out that only 3835 operations were performed for CuCr30 composite due to failure caused by welding, which lead to a lower average welding force of CuCr30 composite under a high current of 25A.

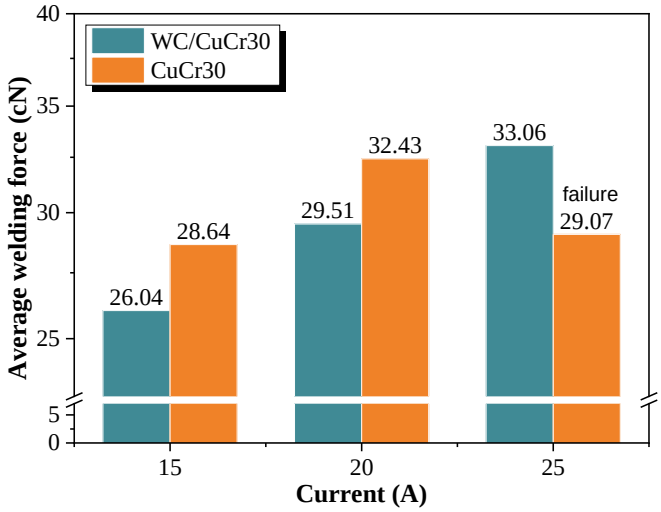

Fig. 11 Average welding force of WC/CuCr30 and CuCr30 composites under different currents.

When the current is low, the local area melts to form a tiny molten pool under lower the arc energy, while the anode and cathode metal vaporization, in the arc electromagnetic force and the role of surface tension stirring at the same time caused by local droplet spatter, the material from the cathode to the anode all transfer occurs. When the current is higher, the heat accumulation on the contact surface intensifies the metal vaporization process under the higher the arc energy. In addition, the increase in electric field strength between the cathode and anode indirectly increases the arc electromagnetic force, which in turn leads to the contact cathode droplet spraying into the surrounding environment, and the contact loss is more obvious. During mass transfer, droplets spattered from the cathode are oxidized in air, which can lead to excess mass transfer by depositing more mass at the anode than is lost at the cathode [26-28].

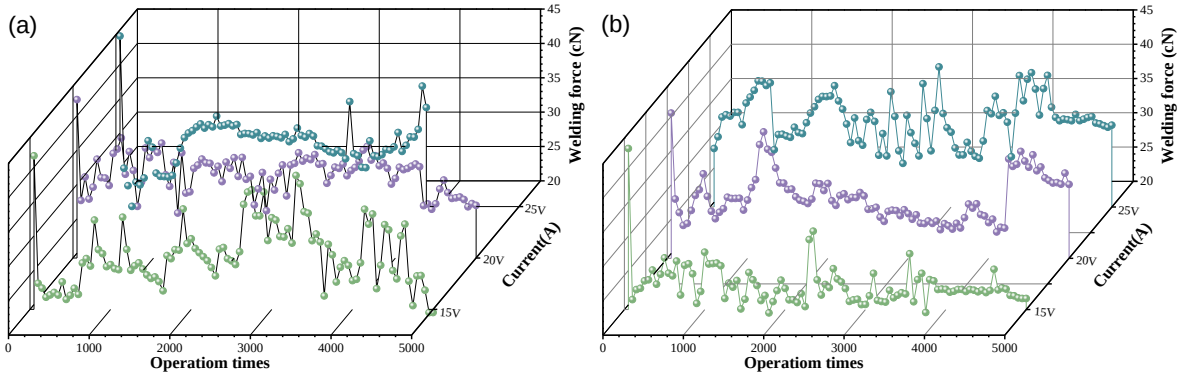

Fig. 12 Welding force variation of composites against operation times under different currents.
(a) CuCr30, (b) WC/CuCr30

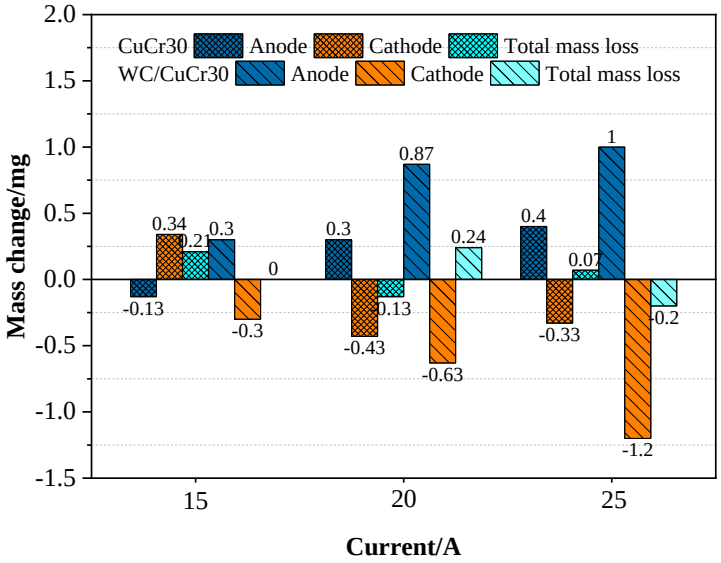

Fig. 13 Mass change of WC/CuCr30 and CuCr30 composites under different currents

3.2.3 Arc erosion morphologies and analysis

Fig.14 and Fig.15 show the cathodic and anodic arc erosion morphologies of WC/CuCr30 and CuCr30 composites under different currents, respectively. As seen in Fig.14, the cathodic erosion surface on CuCr30 composite is obviously more rough and uneven than that on WC/CuCr30 composite. At low current of 15 A and 20A, the erosive areas of WC/CuCr30 composite are smaller and smoother than those of CuCr30 composite, and large erosion pits can be seen on the erosive area on surface of CuCr30 composite, which is mainly due to mass transfer during the arc erosion process. Fig.15 shows the anodic erosion morphologies of WC/CuCr30 and CuCr30 composites under different currents, respectively. As seen, the erosion area of WC/CuCr30 and CuCr30 composites are basically the same, while there are more obvious erosion pits and ablation marks on the surface of CuCr30 composites. When the current increased to 25 A, the number of CuCr30 composite operation was only 3835 times, so the erosion had little change compared with that of 20 A. The erosion area of WC/CuCr30 composite increases with the increase of current. There are serious bumps on the anode erosion surface of CuCr30 than that of WC/CuCr30 composites, and large ablation pits in the erosion center of the cathode (Fig.14(c_1)). Combined with Fig.12, the addition of WC particles and nano-Cr precipitation can not only extend contact life of CuCr material,

but also be helpful to disperse the arc to avoid concentrated erosion. In addition, Cr and WC particles with high melting point increase the motion resistance of molten metal, which reduces the emission number and size of droplets and particles on the surface of the contact during arc erosion, and reduces the density of metal vapor, thus improving the breaking ability of the contact material.

Welding is one of the main forms of contact failure. During the contact process, the formation of arc makes the metal on the surface of the cathode and anode contacts melt and form welding. Research found that the melting point, latent heat of melting, latent heat of vaporization and thermal conductivity of the contact material are directly proportional to the welding resistance [29-31]. In addition, the arc energy also has a certain influence on the welding performance of the contact. The arc energy input to the surface of the contact could be expressed as follow [29],

$$W = \int_0^{t_a} ui\, dt \tag{3}$$

Where, W is arc energy, i is arc current, u is arc voltage and t_a is arc duration. The arc action on the contact surface will cause macroscopic effects such as temperature rise, phase transition (evaporation, melting, etc.) and droplet spatter. These effects will consume arc energy, cause the change of the surface microstructure of the contact, and then make the contact welding. Therefore, the energy consumed per unit mass can be expressed as the following formula,

$$w=\int_{T_0}^{T} C_P\, dT + H_m + H_v + Q_r \tag{4}$$

Where, $\int_{T_0}^{T} C_P\ dT$ is heat enthalpy, which represents the arc energy absorbed by the temperature rise of the contact surface; C_P is the specific heat of constant pressure; H_m is the latent heat of melting, representing the arc energy absorbed by the contact material per unit mass during melting. H_v is the latent heat of vaporization, representing the arc energy absorbed when the contact material evaporates; Q_r is the energy consumed by the oxide decomposition reaction.

$$\int_0^{t_a} ui\, dt = m(\int_{T_0}^{T} C_P dT + H_m + H_v + Q_r) \tag{5}$$

Where, m is the mass of the material where the thermal effect occurs. The larger the load current, the longer the arc duration, the greater the arc energy input to the contact surface, the higher the temperature rise of the contact surface, and the more possibility of contact welding.

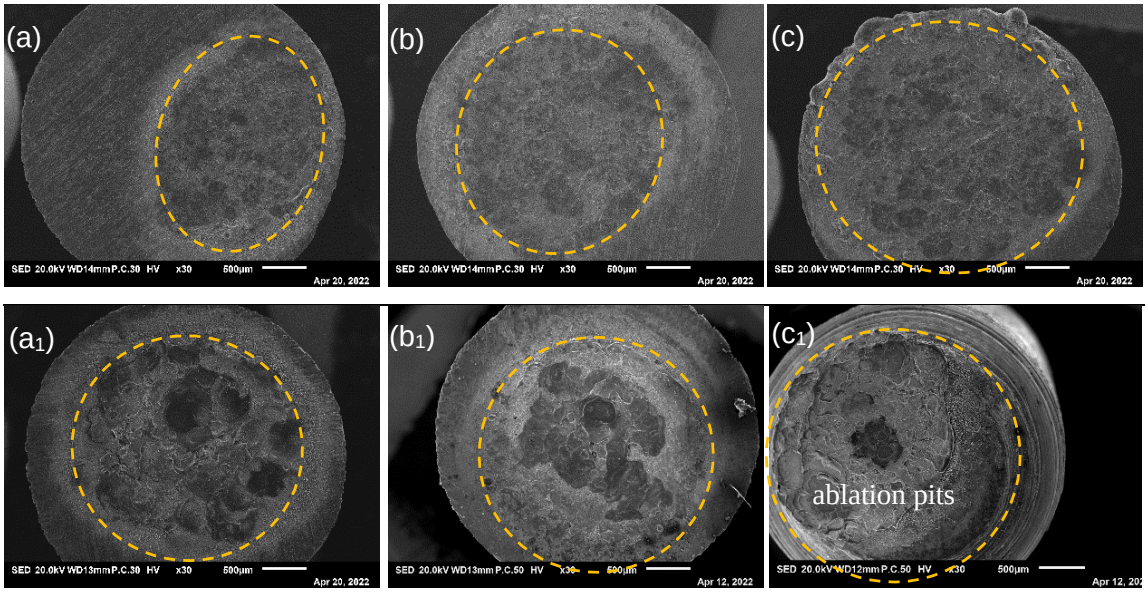

Fig.14 Cathodic erosion morphologies of WC/CuCr30composite(a-c) and CuCr30 composite(a1-c1) under

different current. (a)(a_1) 15A; (b)(b_1) 20A; (c)(c_1) 25A.

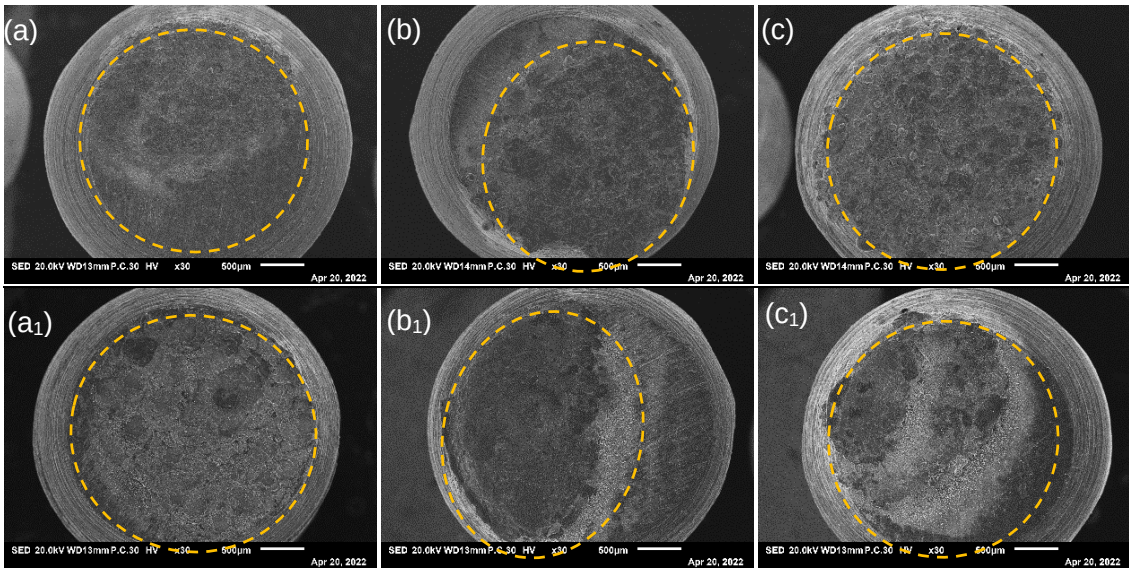

Fig.15 Anodic erosion morphologies of WC/CuCr30composite(a-c) and CuCr30 composite(a_1-c_1) under different current: (a)(a_1) 15A; (b)(b_1) 20A; (c)(c_1) 25A.

Fig. 16 shows the amplified morphologies and corresponding energy spectrum analysis of typical arc erosion morphologies of WC/CuCr30 composite. The results show that mark A1 and A2 on anode of WC/CuCr30 composite are coral structure and its roots. The high O content in the coral structures (Fig. 16(a)) indicates that atmospheric oxygen is dissolved in the coral structures. During arc erosion, vaporization and liquid evaporation sputtering effects result in the absorption of large amounts of oxygen in gaseous Cu or tiny Cu droplets. Previous research showed that CuO and Cu_2O can be found on the surface of copper matrix contacts [32]. And for WC/CuCr30 composite, the high O content in the coral structure further confirms the existence of oxidation. Fig.16(b) shows the amplified morphologies of cathode of WC/CuCr30 composite. As seen, there are droplets, skeletons, and pores on the erosion surface. The bumps (Mark B3) are mainly formed by the Cu droplets sputtered in the arc erosion process. The formation of pores is mainly due to the escape of gas from the melt pool as the temperature decreases, and the holes are mainly formed by the aggregation of pores. As seen in Mark B1 and B2, except for the matrix Cu phase and oxidation phase, the skeletons mainly consist of a Cr phase. In the service of high-temperature, Cr and O show a huge affinity, promoting the formation of Cr_2O_3 and significantly improving the anti-oxidation performance. At the same time, the presence of Cr_2O_3 can also increase the contact resistance of the contact [21]. It is worth mentioned that there are a small amount of W element and C element found in the energy spectrum, that is because the presence of WC particles. At high temperatures, WC decomposes into tungsten and carbon, and the W element is oxidized by air into WO, further increasing the content of O element and contact resistance of the material.

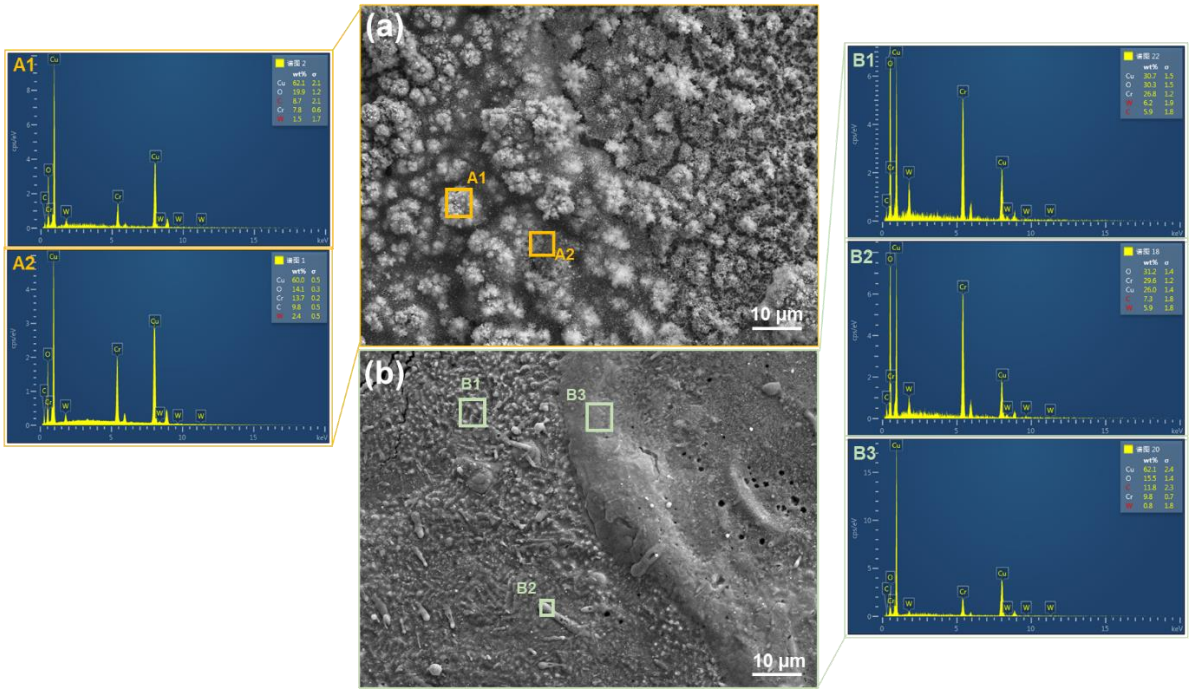

Fig.16 EDS analysis on erosion morphologies of WC/CuCr30composite (a) anode; (b) cathode

3.3 Mechanism of arc erosion resistance

Recent studies have demonstrated that the Cr phase in CuCr contact materials is the preferred attachment point of cathode arc for it belongs to the weak current dielectric phase [32,33]. Fig.17 shows a schematic diagram of erosion mechanism of WC/CuCr30 composites. For CuCr30 composite without WC addition and nano-Cr precipitation, arc trajectory along electron emission site is shown in the red arrow in the Fig.17(a), and arc erosion is concentrated within the red dotted box, which is easy to lead to concentrated arc erosion. In the WC/CuCr30 composite, the precipitation of nano-Cr increases the preferential electron emission sites of Cr phase under the action of applied electric field. Consequently, the arc diffusion follows the direction of the red arrows, and arc erosion expands to large area (Fig.17(b)). Therefore, the precipitation of nano-Cr in WC/CuCr30 composite can promote the motion of cathode arc and accelerate the arc dispersion efficiency. Arc discharge is not concentrated in a local area. Instead, it can spread to a larger area as far as possible to reduce the deterioration of arc erosion performance. As seen in Fig.14, the precipitation of nano-Cr can delay the formation of bumps and pits in the erosion morphology by reducing the arc energy concentration of Cr phase. The presence of $Cr_{23}C_6$ phase around the WC particles effectively improves the interfacial bonding between Cu and WC phases and reduces the chance of pores at the interface. In the process of arc ablation, the pore easily becomes the anchor position of arc root, so that the cathode arc stays for a long time, thus forming rapid local ablation. Secondly, the gas released by the pores in the process of high-temperature arc breakdown will affect the vacuum degree in the arc extinguishing chamber, resulting in a sharp deterioration of the vacuum circuit breaker performance, which is especially easy to occur in the process of multiple large current breaks [34,35]. In addition, as WC particles are uniformly dispersed in the copper matrix, these particles strengthen the Cu matrix to a certain extent. Meanwhile, the Cr becomes the weak electric dielectric phase in the WC/CuCr30 composite. It was reported that the addition of WC particles increased the molten pool's viscosity, decreased the flow of Cu during the arc erosion process, stabilized the WC/CuCr30 composite's microstructure uniformity, and

further enhanced the arc erosion resistance of the material [27].

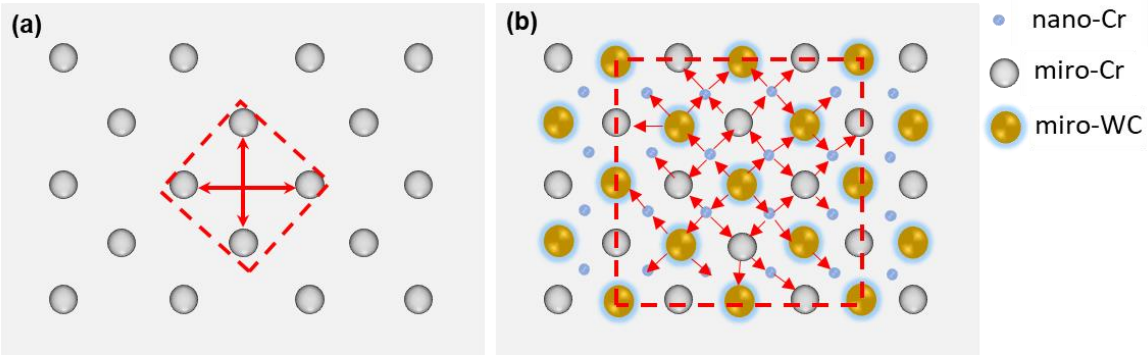

Fig. 17. Schematic diagram of arc spread path. (a)CuCr30; (b) WC/CuCr30

4 Conclusion

(1) WC/CuCr30 composite with uniform and dense microstructure was prepared by spark plasma sintering (SPS). The nano-Cr phase precipitated in copper matrix can effectively improve the interfacial bonding strength between the Cu matrix and WC particles, and part of the precipitated nano-Cr phase combines with the C element in WC to form nano-$Cr_{23}C_6$. Both nano phases can improve the resistance of dislocation and sub-grain boundary movement in the deformation process of WC/CuCr30 composite, thus improving the hardness of copper matrix with a light electrical conductivity decrease.

(2) The addition of WC particles and nano-Cr precipitation can not only extend contact life of CuCr material, but also be helpful to disperse the arc to avoid concentrated erosion. In addition, Cr and WC particles with high melting point increase the motion resistance of molten metal, thus improving the breaking ability of the contact material.

(3) The precipitation of nanometer Cr in WC/CuCr30 composite can promote the motion of cathode arc, disperse the arc erosion, and reduce the deterioration of arc erosion. The presence of $Cr_{23}C_6$ phase around WC particles effectively reduces the probability of pore existence at the interface, which is beneficial to vacuum breaking performance.

Author Statement

We declare that we have no financial and personal relationships with other people or organizations that can inappropriately influence our work, and there is no professional or other personal interest of any nature or kind in any product, service, and/or company that could be construed as influencing the position presented in, or the review of, the manuscript entitled.

Declaration of Competing Interest

The authors declare that they have no known competing financial interests or personal relationships that could have appeared to influence the work reported in this paper.

Acknowledgment

This work was supported by Science and Technology R&D Plan Joint Fund of Henan Province (225200810052), National Natural Science Foundation of China (52071133), Zhongyuan Scholar Workstation Funded Project (214400510028, 224400510025), Key R & D and promotion projects of Henan Province (222102230064), R & D Projects of Henan Academy of Sciences (220910009).

References

[1] P.G. Slade, The Vacuum Interrupter Theory, Design, and Application (2nd ed.), CRC Press, Boca Raton, 2020.

[2] L. Varoto, M. Chosson, J.J. Blandin, A. Papillon, S. Roure, G. Martin, I.O.P. Publ, Microstructural evolutions induced by an electrical breakdown in a binary Cu-25Cr alloy, 42nd Riso International Symposium on Materials Science - Microstructural Variability - Processing, Analysis, Mechanisms and Properties, Tech Univ Denmark, Dept Civil & Mech Engn, Roskilde, DENMARK, 2022.

[3] S. Liang, M. Zhou, Y. Zhang, S. Liu, X. Li, B. Tian, Y. Geng, Y. Ban, Y. Jia, Y. Liu, A.A. Volinsky, Thermal deformation behavior of GO/CeO_2 in-situ reinforced Cu30Cr10W electrical contact material, Journal of Alloys and Compounds 899 (2022) 163266.

[4] Y. Guo, Y. Sun, A. Tang, C.H. Wang, Y.Q. Zhao, M.M. Bai, S.T. Xu, Z.Q. Xu, T. Tang, S. Wang, C.G. Qiu, K. Xu, X.B. Peng, J.F. Han, E. Pop, Y. Chai, Field-effect at electrical contacts to two-dimensional materials, Nano Research 14(12) (2021) 4894-4900.

[5] Y.L. Chang, W. Zheng, Z.M. Zhou, Y.X. Zhai, Y.P. Wang, Preparation and Performance of Cu-Cr Contact Materials for Vacuum Switches with Low Contact Pressure, Journal of Electronic Materials 45(11) (2016) 5647-5654.

[6] H.T. Wang, Q.L. Cai, J.Q. Wang, Y. Zhang, D.K. Hu, Y.L. Wang, First-principles and experimental investigations on physical properties and arc erosion behavior of metal-doped $AgSnO_2$ electrical contact materials, Ceramics International 49(15) (2023) 26033-26048.

[7] X.H. Zhang, Y. Zhang, B.H. Tian, J.C. An, Z. Zhao, A.A. Volinsky, Y. Liu, K.X. Song, Arc erosion behavior of the Al_2O_3-Cu/(W, Cr) electrical contacts, Composites Part B-Engineering 160 (2019) 110-118.

[8] H. Li, X. Wang, Z. Hu, X. Guo, Investigation on arc behavior of AgNi electrical contact material with three-dimensional network structure, Vacuum 175 (2020) 109290.

[9] W. An, Z.-h. Dou, J.-r. Han, T.-a. Zhang, Microstructure uniformity control of CuCr alloy prepared in-situ by aluminothermic reduction coupled with permanent magnetic stirring, Journal of Alloys and Compounds 960 (2023) 170797.

[10] J.P. Zhang, X.M. Feng, Y.F. Shen, C. Chen, C.Y. Duan, Microstructures and properties of Cu-Cr-W composite coatings fabricated by surface mechanical alloying technique, Rare Metals 41(12) (2022) 4248-4256.

[11] S.L. Liang, S. Liu, Y. Zhang, M. Zhou, B.H. Tian, Y.F. Geng, Y. Liu, Y.L. Jia, X. Li, A.A. Volinsky, Effect of in situ graphene-doped nano-CeO_2 on microstructure and electrical contact properties of Cu30Cr10W contacts, Nanotechnology Reviews 10(1) (2021) 385-400.

[12] J.R. Han, Z.H. Dou, T.A. Zhang, W. An, Effect of reduction-slagging coupling of Cr_2O_3 during in-situ preparation of homogeneous CuCr50 alloy by self-propagating high temperature synthesis metallurgy, Journal of Materials Research and Technology 19 (2022) 3658-3669.

[13] K. Duan, X. Guo, K. Song, X. Wang, J. Feng, S. Li, J. Zhong, K. Li, Influence of WC particles addition on material transfer behavior of CuCr30 contact material, Materials Today Communications 34 (2023) 105058.

[14] Y.L. Chang, W. Zheng, Z.M. Zhou, Y.X. Zhai, Y.P. Wang, Preparation and Performance of Cu-Cr Contact Materials for Vacuum Switches with Low Contact Pressure, Journal of Electronic Materials 45(11) (2016) 5647-5654.

[15] Y.-W. Cho, J.-J. Sim, J.-S. Byeon, T.-S. Kim, K.-A. Lee, H.-J. Ju, S.-J. Seo, K.-T. Park, Comparative Study of the Properties of Cu-Cr-Mo System Electrical Contact Material by Sintering and Infiltration Methods, Metals 11(5)

(2021) 700.
[16] L. Shan, X. Wang, Y. Chang, Y. Wang, Improving the mechanical performance of CuCr alloy by dissolving Cu in the Cr second phase, Materials Characterization 176 (2021) 111104.
[17] L. Zhuo, J. Sun, Q. Zhang, Y. Zhang, S. Liang, Y. Tang, Hierarchical tungsten-copper composite reinforced by a concrete skeleton of particulate and fibrous tungsten with coherent Cr precipitates in the copper matrix, Materials Characterization 184 (2022) 111670.
[18] J. Feng, K. Song, S. Liang, X. Guo, Y. Jiang, Electrical wear of TiB_2 particle-reinforced Cu and Cu–Cr composites prepared by vacuum arc melting, Vacuum 175 (2020) 109295.
[19] M. Dias, N. Pinhão, R. Faustino, R.M.S. Martins, A.S. Ramos, M.T. Vieira, J.B. Correia, E. Camacho, F.M. Braz Fernandes, B. Nunes, A. Almeida, U.V. Mardolcar, E. Alves, New WC-Cu composites for the divertor in fusion reactors, Journal of Nuclear Materials 521 (2019) 31-37.
[20] Y.M. Xie, X.C. Meng, Y.X. Huang, J.C. Li, J. Cao, Deformation-driven metallurgy of graphene nanoplatelets reinforced aluminum composite for the balance between strength and ductility, Composites Part B-Engineering 177 (2019).
[21] K.Y. Duan, X.H. Guo, K.X. Song, X. Wang, J. Feng, S.L. Li, J.Y. Zhong, K. Li, Arc erosion resistance of WC/CuCr30 composites based on changing of Cr particle morphology and orientation, Journal of Materials Research and Technology 24 (2023) 9069-9081.
[22] L.P. Deng, K. Han, K.T. Hartwig, T.M. Siegrist, L.Y. Dong, Z.Y. Sun, X.F. Yang, Q. Liu, Hardness, electrical resistivity, and modeling of in situ Cu-Nb microcomposites, Journal of Alloys and Compounds 602 (2014) 331-338.
[23] C. Wu, D. Yi, W. Weng, S. Li, J. Zhou, F. Zheng, Arc erosion behavior of Ag/Ni electrical contact materials, Materials & Design 85 (2015) 511-519.
[24] Y. Liu, X. Wang, H. Li, J. Lu, Z. Wang, C. Zhou, Enhancing properties of $AgTiB_2$ contact material by CuO semi-coated TiB_2 composite particles, Materials Letters 293 (2021) 129703.
[25] H. Li, X. Wang, Z. Hu, Y. Qiu, Effect of Ni addition on the arc-erosion behavior of Ag-4 wt.%SnO_2 electrical contact material, Journal of Alloys and Compounds 829 (2020) 154487.
[26] W. Guan, J. Yuan, H. Lv, T. Zhu, Y. Fang, J. Liu, H. Wang, Z. Li, Z. Tang, W. Yang, Homogeneous arc ablation behaviors of CuCr cathodes improved by chromic oxide, Journal of Materials Science & Technology 81 (2021) 1-12.
[27] X.H. Guo, K.Y. Duan, X. Wang, K.X. Song, X.F. Zhang, K. Li, Thermal and arc erosion behavior of CuCr contact material based on large plastic deformation treatment, Journal of Materials Research and Technology, 23 (2023) 348-358.
[28] J. Duan, X. Guo, J. Feng, X. Wang, K. Qi, H. Song, K. Song, Study on the arc erosion resistance and mechanism of Cr- doped WCu composites, Materials Characterization, 205 (2023) 113291.
[29] L. Yu, Y. Geng, Q. Li, J. Wang, Z. Liu, D. Li, W. Wang, X. Wang, Improvement of Percussion Welding Characteristics of CuCr25 Contact Material by Decreasing Tensile Strength, 2009 Proceedings of the 55th IEEE Holm Conference on Electrical Contacts, 2009, pp. 197-201.
[30] S. Liang, Y. Li, Y. Zhang, M. Zhou, S. Liu, X. Li, Y. Geng, B. Tian, Y. Jia, Y. Liu, A.A. Volinsky, Mechanical and electrical properties of Cu30Cr0.2Zr composites enhanced by CeO_2/GO, Journal of Alloys and Compounds 934 (2023) 167759.
[31] S. Liu, L. Li, M. Zhou, S. Liang, Y. Zhang, J. Huang, B. Tian, Y. Geng, Y. Liu, Y. Jia, X. Li, A.A. Volinsky,

Preparation and properties of graphene reinforced Cu/0.5$CeO_2$30Cr electrical contact materials, Vacuum 195 (2022) 110687.
[32] W. An, Z.-h. Dou, J.-r. Han, T.-a. Zhang, Microstructure evolution and property strengthening of CuCr50 prepared by thermite reduction-electromagnetic casting during the heat treatment process, Journal of Materials Research and Technology 24 (2023) 6533-6544.
[33] H. Li, X. Wang, Y. Liu, X. Guo, Effect of strengthening phase on material transfer behavior of Ag-based contact materials under different voltages, Vacuum 135 (2017) 55-65
[34] J. Duan, X. Guo, T. Huang, K. Song, J. Feng, X. Wang, J. Zhong, K. Duan, Y. Zhang, Arc ablation resistance behavior of Cu-W alloys with different W contents under atmospheric environment, Materials Today Communications 34 (2023) 105173.
[35] X. Wang, S. Liang, P. Yang, Z. Fan, Effect of Al_2O_3 particle size on vacuum breakdown behavior of Al_2O_3/Cu composite, Vacuum 83(12) (2009) 1475-1480.